Research Square

Preprints are preliminary reports that have not undergone peer review.
They should not be considered conclusive, used to inform clinical practice,
or referenced by the media as validated information.

A novel defined necroptosis-associated gene signature for predicting the prognosis of hepatocellular carcinoma

Yiming Li
Zhongshan Hospital of Xiamen University
Wenxiang Chen
Zhongshan Hospital of Xiamen University
Yu Wang
Zhongshan Hospital of Xiamen University
Jun He
Zhongshan Hospital of Xiamen University
Jianyin Zhou (zhoujianyin2000@sina.com)
Zhongshan Hospital of Xiamen University

Research Article

Keywords: tumor immune infiltration, prognostic, hepatocellular carcinoma, necroptosis, subtype, machine learning, prognostic

Posted Date: March 21st, 2022

DOI: https://doi.org/10.21203/rs.3.rs-1460494/v1

License: This work is licensed under a Creative Commons Attribution 4.0 International License.
Read Full License

Abstract

Background

Hepatocellular carcinoma (HCC) is a highly heterogeneous disease with a poor prognosis and insignificant immunotherapeutic effects. This project attempted to identify new potential biomarkers for necroptosis-associated genes to predict prognosis and improve the situation.

Method

The mRNA expression profiles of HCC patients and their clinical data were downloaded from public databases. Finding differential signature genes (DSGs) after subtyping patients according to the necroptosis-related genes. Gene set enrichment analysis was used to conduct GO terms and KEGG pathways. DSGs were analyzed in TCGA cohort to build a predictive model. Validation was performed on HCC patients from ICGC cohort. The model was evaluated using Kaplan–Meier analysis, time-dependent receiver operating characteristics (ROC), uni-Cox regression, and multi-Cox regression. The immune cell infiltration score and related pathway activity were calculated using single-sample gene set enrichment analysis.

Result

A signature model of necroptosis-associated genes was created. The low-risk group had a more prolonged OS when different risk subgroups were compared. The prognostic model's predictive ability was confirmed by ROC analysis. The risk score was an independent predictor of OS in a multi-Cox analysis. According to functional analysis, immune status differed between the two risk groups. The risk score was significantly related to tumor grade, tumor stage, and immune infiltrate type.

Conclusion

A novel signature made up of four necroptosis-associated genes can be used to predict prognosis and influence immune status in HCC. Furthermore, these genes could be used as immunotherapy targets.

Introduction

Liver cancer ranks sixth in terms of incidence and fourth in mortality among all malignancies, with hepatocellular carcinoma (HCC) accounting for 75–85% of all liver cancer types. HCC is a highly malignant tumor, and early detection and treatment are critical to improving survival rates. Currently, surgery is the only curative treatment for HCC, but only a small percentage of patients have access to it [1]. As a result, research into non-surgical treatment methods is critical.

There have been breakthroughs in the non-surgical treatment of HCC in recent years, and the emergence of immune checkpoint inhibitors (ICIs) (e.g., drugs targeting PD-L1, PD-1, and CTLA4) has given patients new hope. However, the clinical application of related medications remains far from satisfactory [2]. Less than half of patients are sensitive to ICI treatment, and drug complications are unavoidable. New approaches to immunotherapy clinical application are desperately required.

Necroptosis is a form of programmed inflammatory cell death that is distinctly different from other types of programmed cell death (e.g., ferroptosis and pyroptosis) [3 4 5]. The canonical necroptotic pathway includes RIPK1-RIPK3-MLKL[6 7]. An oligomeric complex containing FADD, caspase-8, and caspase-10 recruits active RIPK1. When drugs or viruses inhibit caspase-8 activity, the ligation of TNFR family proteins (including TNFR, FAS, TRAILR, and DR6) recruits and phosphorylates RIPK3 via RIPK1, which then phosphorylates MLKL, resulting in MLKL oligomerization. The oligomerized MLKL transfers to the plasma membrane, causing it to rupture [6 7 8 9]. It was recently discovered that signaling pathways bypass ripk1-mediated upstream activation signals to cause necroptosis. Proteins with RHIM structural domain (e.g., Z-DNA binding protein 1, ZBP1) and TRIF can bind to the RHIM structural domain of RIPK3, resulting in RIPK3 phosphorylation [10 11]. TLR3 and TLR4 are activated in macrophages by double-stranded RNA (dsRNA) and LPS, followed by RIPK3 activation via TRIF [11].

The role of necroptosis in the clinical treatment of HCC has received little attention. As a result, by screening necroptosis-related genes (NRG), we hope to develop an effective genetic marker to indicate prognosis and guide clinical treatment, as well as investigate the relationship between necroptosis and tumor immune microenvironment.

Materials And Methods

Datasets

RNA-seq data and clinicopathological information from 425 HCC samples, including 375 cancer and 50 para-cancer samples, were downloaded from TCGA website until November 15, 2021 (https://portal.gdc.cancer.gov/repository). The external validation cohort's RNA-seq data and clinical information were obtained from ICGC portal (https://dcc.icgc.org/projects/LIRI-JP).

NRGs unsupervised clustering analysis

In total, 14 necroptosis-related genes (NRGs) were identified in literature and are listed in Supplementary Table S1 [3 4 5 6 7 8 9 10 11]. These genes were chosen because they play an important role in necroptosis and overlap less with other types of programmed cell death. The difference in NRG expression between HCC and normal tissues was determined using "LIMMA" packages (* if $P < 0.05$, ** if $P < 0.01$, and *** if $P < 0.001$). R package "ConsensusClusterPlus" was then used for clustering analysis to categorize patients into distinct molecular subtypes based on DNRG. The clustering was done using the following criteria. First, the cumulative distribution function (CDF) gradually and smoothly increased. Second, there were no

groups with a small sample size. Finally, clustering increased intra-group correlation while decreasing inter-group correlation. The analysis was repeated 1000 times to ensure clustering accuracy.

Development and validation of the prognostic model

To assess the prognostic value of DSGs, we used uni-Cox regression analyses, LASSO-Cox analyses, and multi-Cox analyses to build a predictive model. TCGA-HCC patients were divided into low- and high-risk subgroups based on the median risk score and then subjected to a Kaplan–Meier survival analysis. Following that, PCA, t-SNE, and ROC analysis were carried out. An HCC cohort from ICGC database was divided into low- and high-risk groups in the validation studies. The expression of each DSG was also normalized using the "scale" function, and the risk score was computed using the same formula as for TCGA cohort.

Independent prognostic analysis of the risk score

We obtained clinical information from patients in TCGA and ICGC cohorts. In our regression model, the clinical characteristics were analyzed with the risk score. For the analysis, univariate and multivariable Cox regression models were used.

Functional enrichment analysis

We used "LIMMA" R package to compare DSGs from different NRG clusters ($P \leq 0.001$). Then, using these DSGs as a foundation, GO and KEGG analyses were performed using "clusterProfiler" package to investigate the biological functions of DSGs. The infiltration scores of 16 immune cells and the activities of 13 immune-related pathways between the high- and low-risk groups were calculated using ssGSEA with "GSVA" R package.

Statistical analysis

The Wilcoxon test was used when comparing two groups, and when comparing more than two groups, the Kruskal-Wallis test was used. The categorical variables were compared using the Pearson chi-square test. To perform survival analyses, we used the Kaplan-Meier method with a two-sided log-rank test. We used univariate and multivariate Cox regression models to assess the risk model's independent prognostic value. The Mann-Whitney test was used to compare the ssGSEA scores of immune cells or immune pathways between high- and low-risk groups. A two-tailed $P < 0.05$ was used to define statistical significance.

Results

Identification of differentially expressed necroptosis-related genes (DNRG)

Nine DNRGs were identified in TCGA-HCC cohort by comparing the expression levels of 14 NRGs in HCC and paired cancer samples. Three of these genes (FAS, TLR3, and TLR4) were down-regulated in the

tumor, while the remaining six (CASP10, CASP8, TNFRSF21, FADD, MLKL, and RIPK1) were up-regulated (Fig. 1A).

Tumor classification based on DNRGs

The expression of nine DNRGs was used to investigate the relationship between DNRGs and HCC subtypes. The unsupervised cluster analysis was performed on HCC patients in TCGA cohort in conjunction with survival data. By increasing the clustering variable (k) from 2 to 10, we established that when k = 3, the principle of minimal crossover between cluster strata was met, dividing HCC patients into three separate subgroups (Figs. 1B, C).

The differences in DSG expression profiles and clinical characteristics (age, grade, gender, stage, T, N, and M) across different sub-clusters are depicted in Supplementary Figure A. While there was little difference in clinical characteristics (except for tumor grading) between the other clusters, gene expression profiles revealed significant differences. A comparison of OS revealed substantial disparities in survival between clusters (Fig. 1D). To further investigate the differences between various NRGs clusters, "LIMMA" R package was used to search for shared differentially expressed genes between different NRGs clusters (Fig. 1E). These differentially expressed shared genes are referred to as differential signature genes (DSGs).

The GO functional and KEGG pathway enrichment analyses found that DSGs were associated with metabolic pathways and inflammatory cell chemotaxis were consistent, and numerous results pointed to peroxisome-related pathways (Supplementary Figures B, C, D, and E).

Development of DSGs signatures scoring system

In TCGA-HCC cohort, 370 samples had matching survival information. In total, 278 DSGs were screened for significant associations with prognosis using univariate Cox proportional hazard regression analysis to examine the relationship between DSG expression levels and OS in HCC patients (Supplementary Table S2). Following primary filtering, a LASSO-penalized Cox analysis was used to narrow down DSGs expression profiles further (Supplementary Figures F and G). A total of 13 genes were obtained, and a prognostic model was built using multivariate Cox proportional hazards regression analysis (Table 1).

The risk score is calculated as follows:

$$\text{Risk score} = \sum_i^n coef_i * Exp_i,$$

Where coef denotes the contribution of a gene to prognostic risk scores derived from the regression coefficient of multivariate Cox analysis, and Exp indicates the corresponding gene expression level.

Table 1
the results of the multivariate Cox regression analysis between gene expression and OS.

id	coef	HR	HR.95L	HR.95H	p-value
GOT2	-0.27104	0.762583	0.606415	0.958969	0.020432
LDHA	0.481783	1.618959	1.277076	2.052366	6.87E-05
MTHFS	-0.25587	0.774244	0.628165	0.954294	0.016462
BOD1	0.516428	1.676031	1.160734	2.420089	0.005866

The 370 patients were divided into high- and low-risk subgroups based on the median risk score. The results of PCA and t-SNE were consistent, with patients in different risk subgroups well divided into two types (Figs. 2A, B). Patients with a high risk of death died sooner than those with a low risk (Figs. 2C, D). The Kaplan-Meier curve consistently showed that patients in the high-risk group had a significantly shorter life expectancy than their low-risk counterparts (Fig. 2E).

The sensitivity and specificity of the prognostic model were assessed using ROC analysis, and the results revealed that the areas under the ROC curve (AUC) for one, three, and five-year survival were 0.742, 0.720, and 0.713, respectively (Fig. 2F).

Validation of the prognostic model in the ICGC cohort

The prognostic model's robustness was evaluated using HCC patients from ICGC cohort. The ICGC cohort's risk scores were calculated using the formula described above. The TCGA cohort's median risk score was used as the risk cutoff to divide the ICGC cohort into high- and low-risk subgroups. The findings were comparable to those obtained from TCGA cohort. PCA and t-SNE analyses confirmed that the two subgroups of patients were significantly different (Figs. 3A, B). Similarly, patients in the high-risk group lived for a shorter period than those in the low-risk group (Figs. 3C, D, and E). Furthermore, AUC values at one, three, and five years were 0.725, 0.674, and 0.568, respectively (Fig. 3F).

Relationship between prognostic models and clinicopathological parameters

Univariate and multivariate Cox regression analyses were performed on the available variables to determine whether the risk scores derived from the prognostic models could be used as independent prognostic predictors for patients with HCC (Table 2). In univariate Cox regression analyses, a risk score was significantly associated with OS in both the TCGA and the ICGC cohorts (TCGA cohort: $P < 0.001$; ICGC cohort: $P < 0.001$; Supplementary Figures H, I). According to multivariate Cox regression analysis, stage and risk score are independent risk factors associated with OS (TCGA cohort: $P < 0.001$; ICGC cohort: $P < 0.001$; Supplementary Figures J, K). In addition, we created a heatmap of the TCGA cohort's clinical characteristics (Fig. 4A) and discovered that grade, stage, and T were distributed differently between low- and high-risk subgroups (Figs. 4B, C, D; $P < 0.05$).

Table 2
Results of the univariate and multivariate Cox regression analyses regarding OS in the TCGA cohort and the ICGC cohort.

	Uni-Cox				
TCGA	id	HR	HR.95L	HR.95H	pvalue
	age	1.010780211	0.996272454	1.02549923	0.146037802
	gender	0.77472331	0.530779003	1.130783628	0.185858636
	grade	1.124946709	0.874228238	1.447568315	0.360106468
	stage	1.653386261	1.348806121	2.02674505	1.30E-06
	riskScore	1.560433971	1.383725292	1.759709237	3.97E-13
ICGC	gender	0.502131855	0.268152148	0.940273652	0.031367574
	age	1.004027424	0.973299752	1.035725188	0.799923193
	stage	2.202772352	1.518807898	3.194746381	3.14E-05
	riskScore	1.514947864	1.290453407	1.778496626	3.85E-07
	Multi-Cox				
TCGA	stage	1.471163801	1.184259608	1.827574726	0.000486827
	riskScore	1.457229078	1.28356459	1.654390127	6.03E-09
ICGC	gender	0.457515933	0.238156665	0.878920726	0.018904661
	stage	2.006255848	1.373091622	2.931386706	0.000319753
	riskScore	1.350789754	1.112890252	1.63954438	0.002349436

Comparison of the immune activity between subgroups

The first step was to test the correlation between the risk score and immune infiltration to see how it related to the immune component. Recognized studies [12] found six types of immune infiltrates in human tumors: C1 (wound healing), C2 (INF-g dominant), C3 (inflammatory), C4 (lymphocyte depleted), C5 (immunologically quiet), and C6 (immunologically active) (TGF-β dominant). We correlated immune infiltration with the risk score because there is known data on it in the TCGA-HCC cohort. The findings revealed that risk scores were related to immune infiltration. C1 was associated with high-risk scores, while C4 was associated with low-risk scores (Fig. 4E).

ssGSEA was used to calculate the enrichment scores of various immune cell subpopulations, related functions, and pathways to investigate further the relationship between the risk score and immune status. In TCGA cohort, the high-risk group had a higher proportion of aDCs, iDCs, macrophages, Th1 cells, Th2 cells, and Treg cells (Fig. 4F, Supplementary Figure L). In ICGC cohort, similar conclusions were reached.

Among the 13 immune pathways studied, APC co-inhibition, APC co-stimulation, CCR, check-point, HLA, and Type II IFN response were significantly different in TCGA and ICGC cohorts (Fig. 4G, Supplementary Figure M). We investigated whether the risk score was associated with ICI-related biomarkers because ICI is used in clinical practice to treat hepatocellular carcinoma. We chose CD274, CTLA4, HAVCR2, IDO1, LAG3, and PDCD1 [13 14] as immune checkpoint-associated signals and discovered that high-risk scores were positively associated with CTLA4, HAVCR2, LAG3, and PDCD1 expression (Figs. 4H, I, J, K).

Discussion

The role of necroptosis in cancer remains debated. In theory, activating necroptosis in tumor cells could boost anti-tumor immunity. CD8 + T cell activation by dying cells via antigen-presenting cells, results in anti-tumor immunity [15 16]. According to one study, inoculating necrotic, apoptotic cancer cells induced effective anti-tumor immunity in an experimental mouse model [17].

With the advent of next-generation sequencing technology and the era of precision medicine, a new era of tumor therapeutic approaches has emerged [18]. However, there are currently few useful biomarkers in HCC for effective early diagnosis and prediction of therapeutic outcomes. In this study, we attempted for the first time to use necroptosis-associated genes as a predictor of HCC.

Similar to our study, other prognostic models such as the immune-related gene signature and ferroptosis-related gene signature had AUC values of 0.663 and 0.668 for predicting 3-year OS of HCC, respectively [19 20 21 22 23]. The prognostic model of Necroptosis-associated genes developed in our study outperforms the gene signatures described above.

This study screened 14 significant genes related to necroptosis by searching and summarizing previous literature, then systematically analyzed their expression in HCC tissues, yielding nine DNRGs. Although the three clusters formed by the consensus clustering analysis based on DNRGs differed only in tumor grade and gene expression profile, the KM survival analysis revealed significant differences in OS between the three clusters. During the cross-comparison investigation, we discovered 421 genes with differential expression across all three clusters. We believe that these genes are DSGs and that DSGs are the underlying cause of survival differences. The results of GO functional and KEGG pathway enrichment analyses showed that DSGs and peroxisome-related pathways have a close relationship. In patients with non-alcoholic fatty liver disease, PPAR-γ was negatively correlated with hepatic RIPK3 [24]. In one study, the dual peroxisome proliferator-activated receptor alpha/delta agonist elafibranor (ELA) significantly reduced liver lipids and non-alcoholic fatty liver disease activity score in a mouse model via steatosis, inflammation, and fibrosis [25]. In addition, ELA most likely achieves this effect by decreasing necrosis (cleavage of RIP3) and apoptosis (cleavage of caspase 3) in the liver. These findings back up our research direction.

A prognostic model comprised of four DSGs was developed and validated in ICGC cohort to confirm the prognostic value of these DSGs. The findings revealed that tumor grade, stage, and OS differed markedly

between risk subgroups and that independent prognostic analysis revealed that risk score was an independent predictor of OS. This study's prognostic model was made up of four DSGs. Two DSGs (LDHA and BOD1) were up-regulated in HCC tumor tissues, while two DSGs (GOT2 and MTHFS) were down-regulated.

LDHA is a critical glycolytic enzyme. Increased LDHA expression is associated with a poor prognosis in a variety of cancers [26 27]. According to one study, inhibiting LDHA in pancreatic cancer cells had a tumor-suppressive effect [28 29]. Faloppi et al. discovered that patients with advanced pancreatic cancer receiving sorafenib with low LDHA serum levels had a better prognosis [30]. The results of this experiment were also confirmed in breast cancer, where the use of LDHA inhibitors significantly inhibited tumor cell growth and aggressiveness [31]. BOD1 is a protein-coding gene required for cell mitosis, but its role in tumors has received little attention [32]. BOD1 was highly expressed in HCC, and high BOD1 expression was associated with a poor prognosis. Several studies have reached similar conclusions to ours [33]. However, studies on breast cancer revealed that BOD1 deletion destabilizes DNA replication, increasing the likelihood of tumorigenesis. [34]. More research is required to determine the role of BOD1 in cancer. GOT2 catalyzes the reversible interconversion of oxaloacetate and glutamate to aspartate and α-ketoglutarate, which is important in amino acid metabolism and the tricarboxylic acid cycle [35 36]. One study discovered that GOT2 expression was low in HCC and that low GOT2 expression was associated with a poor prognosis. In an in-vitro experiment, increasing GOT2 expression in HCC inhibited tumor cell growth [37]. At the moment, we know very little about MTHFS gene. According to some studies, MTHFS can influence human fatty acid metabolism by influencing DNA methylation [38]. To summarize, the four genes in the prognostic model can help us better understand HCC, but their role require further investigation.

The risk scores of various immune infiltrations differed. This suggests that there could be a link between risk scores and immune microenvironment. It is reasonable to think that necroptosis can influence the composition of tumor immune microenvironment. The immune microenvironment's composition has a significant impact on the efficacy of immune checkpoint inhibitors [39]. Recent advancements in cancer therapy that target immune checkpoints, such as anti-CTLA4 antibodies, have demonstrated effective clinical outcomes [40 41]. The expressions of CTLA4, HAVCR2, LAG3, and PDCD1 were positively correlated with risk scores in our study. Prognostic models can predict immune checkpoint expression levels and potentially guide immunotherapy decisions. According to GSEA analysis, a high-risk score was associated with impaired activity of type II IFN responses, which play an important role in tumor immune surveillance, anti-tumor immunity stimulation, and tumor elimination promotion [42 43 44]. Increased Tfh cells, Treg cells, Th1 cells, Th2 cells, T cell co-stimulation, and T cell co-inhibition in the high-risk group indicated that the immune regulation function was disrupted. According to a recent study, Treg cells suppress anti-tumor immunity and are associated with poor clinical outcomes [45 46]. As a result, it is reasonable to assume that the high-risk group's anti-tumor immunity is diminished, which may be a contributing factor to their poor prognosis.

Even though we used various methods to evaluate our model, there are some drawbacks and shortcomings. It is vulnerable to the biases inherent in this research paradigm because it is a retrospective study. Although immune checkpoint expression levels differed significantly between risk groups, we could not compare the corresponding checkpoint inhibitor IC50s due to a lack of relevant data.

Conclusion

A novel signature made up of four necroptosis-associated genes can be used to predict prognosis and influence immune status in HCC. Furthermore, these genes could be used as immunotherapy targets.

Abbreviations

hepatocellular carcinoma（HCC）; immune checkpoint inhibitors (ICIs); receptor-interacting serine/threonine protein kinase 3 (RIPK3); mixed lineage kinase domain like pseudokinase (MLKL); Fas-associated protein with death domain （FADD）; tumor necrosis factor receptor (TNFR); Z-DNA binding protein 1 (ZBP1); TIR-domain-containing adapter-inducing interferon-β (TRIF); Toll-like receptor 3 (TLR3); double-stranded RNA (dsRNA); lipopolysaccharide (LPS); Necroptosis-related genes (NRGs); differentially expressed Necroptosis-related genes (DNRGs); differential signature genes (DSGs); principal component analysis (PCA); t-distributed stochastic neighbor embedding (t-SNE); Time-dependent receiver operating characteristic (ROC) ; area under the ROC curve (AUC)

Declarations

Competing interests

The authors declare that they have no competing interests.

Funding

This work was supported by the Medical Innovation Project of Fujian Province [2019-CXB-36]; the Natural Science Foundation of Fujian Province [2019J01551]; the Medical and Health Key project of Xiamen (3502Z20191106).

Authors' contributions

All authors participated in the design, interpretation of the studies and analysis of the data and review of the manuscript. Jianyin Zhou and Yiming Li: conceptualization and methodology. Jianyin Zhou and Yiming Li: software and data curation. Jianyin Zhou and Yiming Li: validation. Yiming Li: original draft preparation. Jianyin Zhou and Yiming Li: review, editing, and supervision.

Acknowledgements

The results published here are in part based upon data generated by the TCGA Research Network: https://www.cancer.gov/tcga. TCGA and ICGC data are publicly available. As a result, the current study was exempted from approval by local ethics committees. The present research adheres to TCGA and ICGC data access and publication policies.

References

1. Bray F, Ferlay J, Soerjomataram I, Siegel RL, Torre LA, Jemal A. Global cancer statistics 2018: GLOBOCAN estimates of incidence and mortality worldwide for 36 cancers in 185 countries. *CA Cancer J Clin.*2018;68(6):394-424.
2. Sprinzl MF, Galle PR. Current progress in immunotherapy of hepatocellular carcinoma. *J Hepatol.*2017;66(3):482-484.
3. Bertheloot D, Latz E, Franklin BS. Necroptosis, pyroptosis and apoptosis: an intricate game of cell death. *Cell Mol Immunol.*2021;18(5):1106-1121.
4. Liu ZG, Jiao D. Necroptosis, tumor necrosis and tumorigenesis. *Cell Stress.*2019;4(1):1-8.
5. Najafov A, Chen H, Yuan J. Necroptosis and Cancer. *Trends Cancer.*2017;3(4):294-301.
6. Zhao J, Jitkaew S, Cai Z, et al. Mixed lineage kinase domain-like is a key receptor interacting protein 3 downstream component of TNF-induced necrosis. *Proc Natl Acad Sci U S A.*2012;109(14):5322-5327.
7. Sun L, Wang H, Wang Z, et al. Mixed lineage kinase domain-like protein mediates necrosis signaling downstream of RIP3 kinase. *Cell.*2012;148(1-2):213-227.
8. Chen X, Li W, Ren J, et al. Translocation of mixed lineage kinase domain-like protein to plasma membrane leads to necrotic cell death. *Cell Res.*2014;24(1):105-121.
9. Cai Z, Jitkaew S, Zhao J, et al. Plasma membrane translocation of trimerized MLKL protein is required for TNF-induced necroptosis. *Nat Cell Biol.*2014;16(1):55-65.
10. Upton JW, Kaiser WJ, Mocarski ES. DAI/ZBP1/DLM-1 Complexes with RIP3 to Mediate Virus-Induced Programmed Necrosis that Is Targeted by Murine Cytomegalovirus vIRA. *Cell Host Microbe.*2019;26(4):564.
11. Kaiser WJ, Sridharan H, Huang C, et al. Toll-like receptor 3-mediated necrosis via TRIF, RIP3, and MLKL. *J Biol Chem.*2013;288(43):31268-31279.
12. Thorsson V, Gibbs DL, Brown SD, et al. The Immune Landscape of Cancer. *Immunity.*2018;48(4):812-830.e814.
13. Zhang X, Shi M, Chen T, Zhang B. Characterization of the Immune Cell Infiltration Landscape in Head and Neck Squamous Cell Carcinoma to Aid Immunotherapy. *Mol Ther Nucleic Acids.*2020;22:298-309.
14. Hong W, Liang L, Gu Y, et al. Immune-Related lncRNA to Construct Novel Signature and Predict the Immune Landscape of Human Hepatocellular Carcinoma. *Mol Ther Nucleic Acids.*2020;22:937-947.

15. Snyder AG, Hubbard NW, Messmer MN, et al. Intratumoral activation of the necroptotic pathway components RIPK1 and RIPK3 potentiates antitumor immunity. *Sci Immunol.*2019;4(36).
16. Yatim N, Jusforgues-Saklani H, Orozco S, et al. RIPK1 and NF-κB signaling in dying cells determines cross-priming of CD8 T cells. *Science.*2015;350(6258):328-334.
17. Aaes TL, Kaczmarek A, Delvaeye T, et al. Vaccination with Necroptotic Cancer Cells Induces Efficient Anti-tumor Immunity. *Cell Rep.*2016;15(2):274-287.
18. Morash M, Mitchell H, Beltran H, Elemento O, Pathak J. The Role of Next-Generation Sequencing in Precision Medicine: A Review of Outcomes in Oncology. *J Pers Med.*2018;8(3).
19. Liang JY, Wang DS, Lin HC, et al. A Novel Ferroptosis-related Gene Signature for Overall Survival Prediction in Patients with Hepatocellular Carcinoma. *Int J Biol Sci.*2020;16(13):2430-2441.
20. Dai Y, Qiang W, Lin K, Gui Y, Lan X, Wang D. An immune-related gene signature for predicting survival and immunotherapy efficacy in hepatocellular carcinoma. *Cancer Immunol Immunother.*2021;70(4):967-979.
21. Li Z, Li F, Peng Y, Fang J, Zhou J. Identification of three m6A-related mRNAs signature and risk score for the prognostication of hepatocellular carcinoma. *Cancer Med.*2020;9(5):1877-1889.
22. Chen Q, Li F, Gao Y, Xu G, Liang L, Xu J. Identification of Energy Metabolism Genes for the Prediction of Survival in Hepatocellular Carcinoma. *Front Oncol.*2020;10:1210.
23. Jiang HY, Ning G, Wang YS, Lv WB. Ahypoxia-related signature enhances the prediction of the prognosis in hepatocellular carcinoma patients and correlates with sorafenib treatment response. *Am J Transl Res.*2020;12(12):7762-7781.
24. Wu L, Zhang X, Zheng L, et al. RIPK3 Orchestrates Fatty Acid Metabolism in Tumor-Associated Macrophages and Hepatocarcinogenesis. *Cancer Immunol Res.*2020;8(5):710-721.
25. Briand F, Heymes C, Bonada L, et al. A 3-week nonalcoholic steatohepatitis mouse model shows elafibranor benefits on hepatic inflammation and cell death. *Clin Transl Sci.*2020;13(3):529-538.
26. Brand A, Singer K, Koehl GE, et al. LDHA-Associated Lactic Acid Production Blunts Tumor Immunosurveillance by T and NK Cells. *Cell Metab.*2016;24(5):657-671.
27. Urbańska K, Orzechowski A. Unappreciated Role of LDHA and LDHB to Control Apoptosis and Autophagy in Tumor Cells. *Int J Mol Sci.*2019;20(9).
28. Cui J, Shi M, Xie D, et al. FOXM1 promotes the warburg effect and pancreatic cancer progression via transactivation of LDHA expression. *Clin Cancer Res.*2014;20(10):2595-2606.
29. Zhang D, He Z, Shen Y, Wang J, Liu T, Jiang J. MiR-489-3p Reduced Pancreatic Cancer Proliferation and Metastasis By Targeting PKM2 and LDHA Involving Glycolysis. *Front Oncol.*2021;11:651535.
30. Liu R, Li Y, Tian L, et al. Gankyrin drives metabolic reprogramming to promote tumorigenesis, metastasis and drug resistance through activating β-catenin/c-Myc signaling in human hepatocellular carcinoma. *Cancer Lett.*2019;443:34-46.
31. Jin L, Chun J, Pan C, et al. Phosphorylation-mediated activation of LDHA promotes cancer cell invasion and tumour metastasis. *Oncogene.*2017;36(27):3797-3806.

32. Esmaeeli-Nieh S, Fenckova M, Porter IM, et al. BOD1 Is Required for Cognitive Function in Humans and Drosophila. *PLoS Genet.*2016;12(5):e1006022.
33. Yang H, Li G, Qiu G. Bioinformatics Analysis Using ATAC-seq and RNA-seq for the Identification of 15 Gene Signatures Associated With the Prediction of Prognosis in Hepatocellular Carcinoma. *Front Oncol.*2021;11:726551.
34. Wang L, Collings CK, Zhao Z, et al. A cytoplasmic COMPASS is necessary for cell survival and triple-negative breast cancer pathogenesis by regulating metabolism. *Genes Dev.*2017;31(20):2056-2066.
35. Wang T, Yao W, Li J, He Q, Shao Y, Huang F. Acetyl-CoA from inflammation-induced fatty acids oxidation promotes hepatic malate-aspartate shuttle activity and glycolysis. *Am J Physiol Endocrinol Metab.*2018;315(4):E496-e510.
36. Yang H, Zhou L, Shi Q, et al. SIRT3-dependent GOT2 acetylation status affects the malate-aspartate NADH shuttle activity and pancreatic tumor growth. *Embo j.*2015;34(8):1110-1125.
37. Huang ZL, Huang XY, Huang J, et al. Multiple Omics Integration Reveals Key Circular RNAs in Hepatocellular Carcinoma. *Front Oncol.*2021;11:621353.
38. Pescador-Tapia A, Silva-Martínez GA, Fragoso-Bargas N, et al. Distinct Associations of BMI and Fatty Acids With DNA Methylation in Fasting and Postprandial States in Men. *Front Genet.*2021;12:665769.
39. Myers JA, Miller JS. Exploring the NK cell platform for cancer immunotherapy. *Nat Rev Clin Oncol.*2021;18(2):85-100.
40. Dolladille C, Ederhy S, Sassier M, et al. Immune Checkpoint Inhibitor Rechallenge After Immune-Related Adverse Events in Patients With Cancer. *JAMA Oncol.*2020;6(6):865-871.
41. Cheng AL, Hsu C, Chan SL, Choo SP, Kudo M. Challenges of combination therapy with immune checkpoint inhibitors for hepatocellular carcinoma. *J Hepatol.*2020;72(2):307-319.
42. Wang L, Wang Y, Song Z, Chu J, Qu X. Deficiency of interferon-gamma or its receptor promotes colorectal cancer development. *J Interferon Cytokine Res.*2015;35(4):273-280.
43. Mitra-Kaushik S, Harding J, Hess J, Schreiber R, Ratner L. Enhanced tumorigenesis in HTLV-1 tax-transgenic mice deficient in interferon-gamma. *Blood.*2004;104(10):3305-3311.
44. Street SE, Trapani JA, MacGregor D, Smyth MJ. Suppression of lymphoma and epithelial malignancies effected by interferon gamma. *J Exp Med.*2002;196(1):129-134.
45. Zhou SL, Zhou ZJ, Hu ZQ, et al. Tumor-Associated Neutrophils Recruit Macrophages and T-Regulatory Cells to Promote Progression of Hepatocellular Carcinoma and Resistance to Sorafenib. *Gastroenterology.*2016;150(7):1646-1658.e1617.
46. Zhang Q, He Y, Luo N, et al. Landscape and Dynamics of Single Immune Cells in Hepatocellular Carcinoma. *Cell.*2019;179(4):829-845.e820.

Figures

fig1

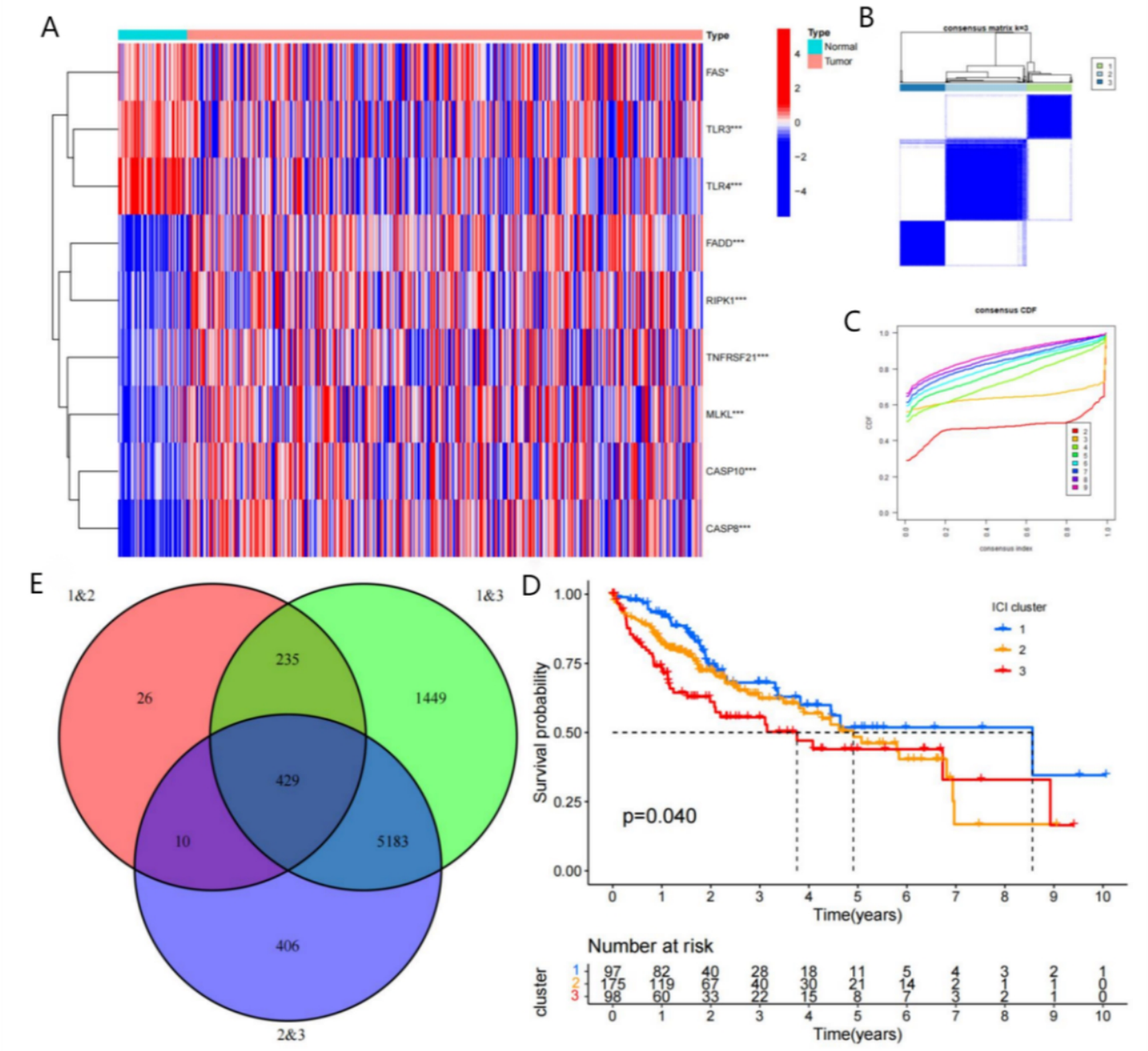

Figure 1

Expressions of 9 DNRGs and Tumor classifification based on the DNRGs

A. Heatmap of the DNRGs between the normal and the tumor tissues. (blue: low expression level; red: high expression level).

B. 370 HCC patients were grouped into two clusters according to the consensus clustering matrix (k = 3).

C. Consensus clustering cumulative distribution function (CDF) when K = 2-9.

D. Kaplan–Meier OS curves for the THREE clusters

E. Common intersection genes, defined as differential signature genes (DSGs), between the three DNRG modification patterns.

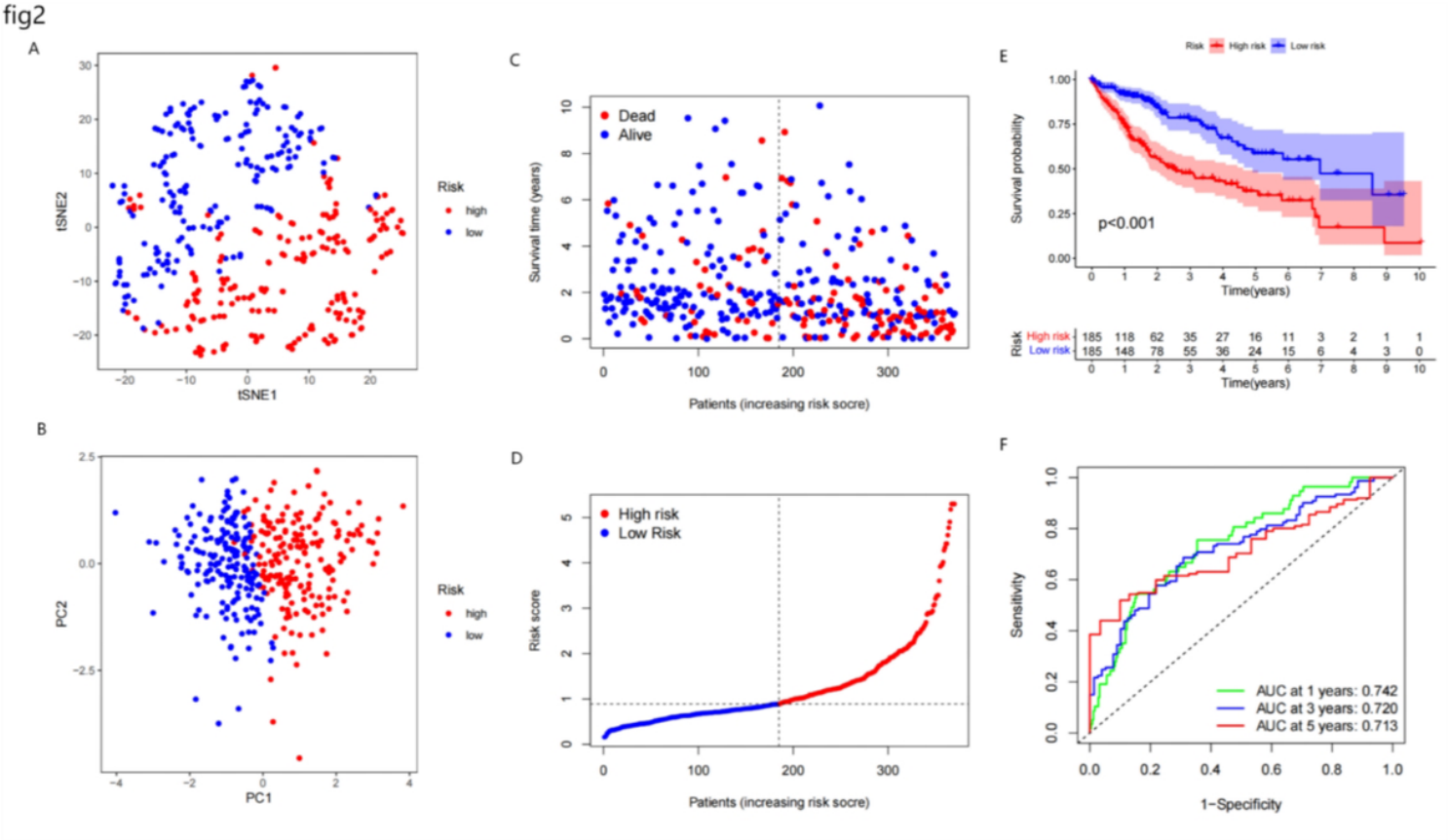

Figure 2

Validation of risk signature in the TCGA cohort.

A, B. PCA and t-SNE plot for HCC patients based on the risk score.

C. The survival status for each patient

D. Distribution of patients based on the risk score.

E. Kaplan–Meier curves for the OS of patients in the high- and low-risk groups.

F. ROC curves demonstrated the predictive efficiency of the risk score.

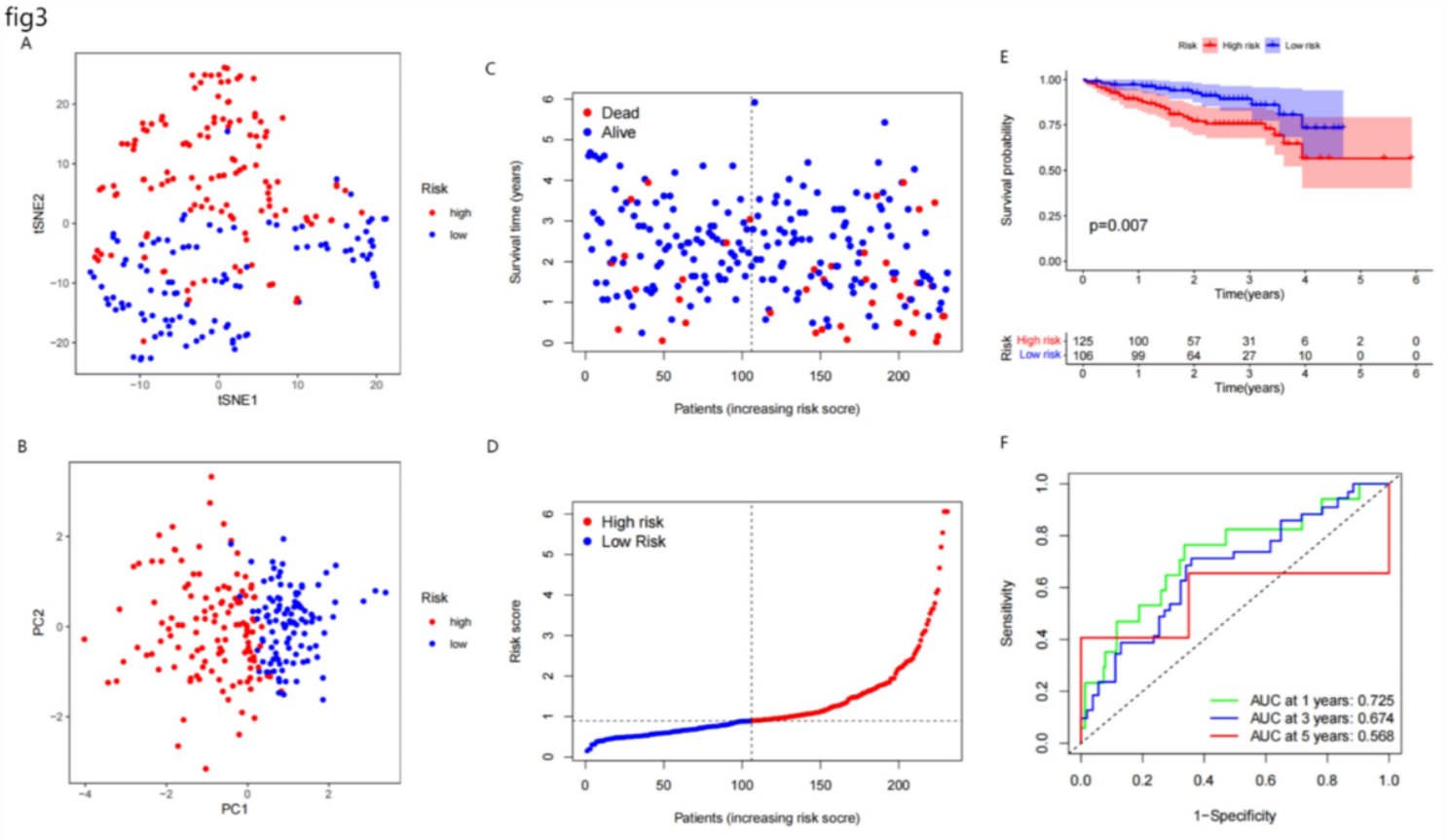

Figure 3

Validation of risk signature in the ICGC cohort.

A, B. PCA and t-SNE plot for HCC patients based on the risk score.

C. The survival status for each patient

D. Distribution of patients based on the risk score.

E. Kaplan–Meier curves for the OS of patients in the high- and low-risk groups.

F. ROC curves demonstrated the predictive efficiency of the risk score.

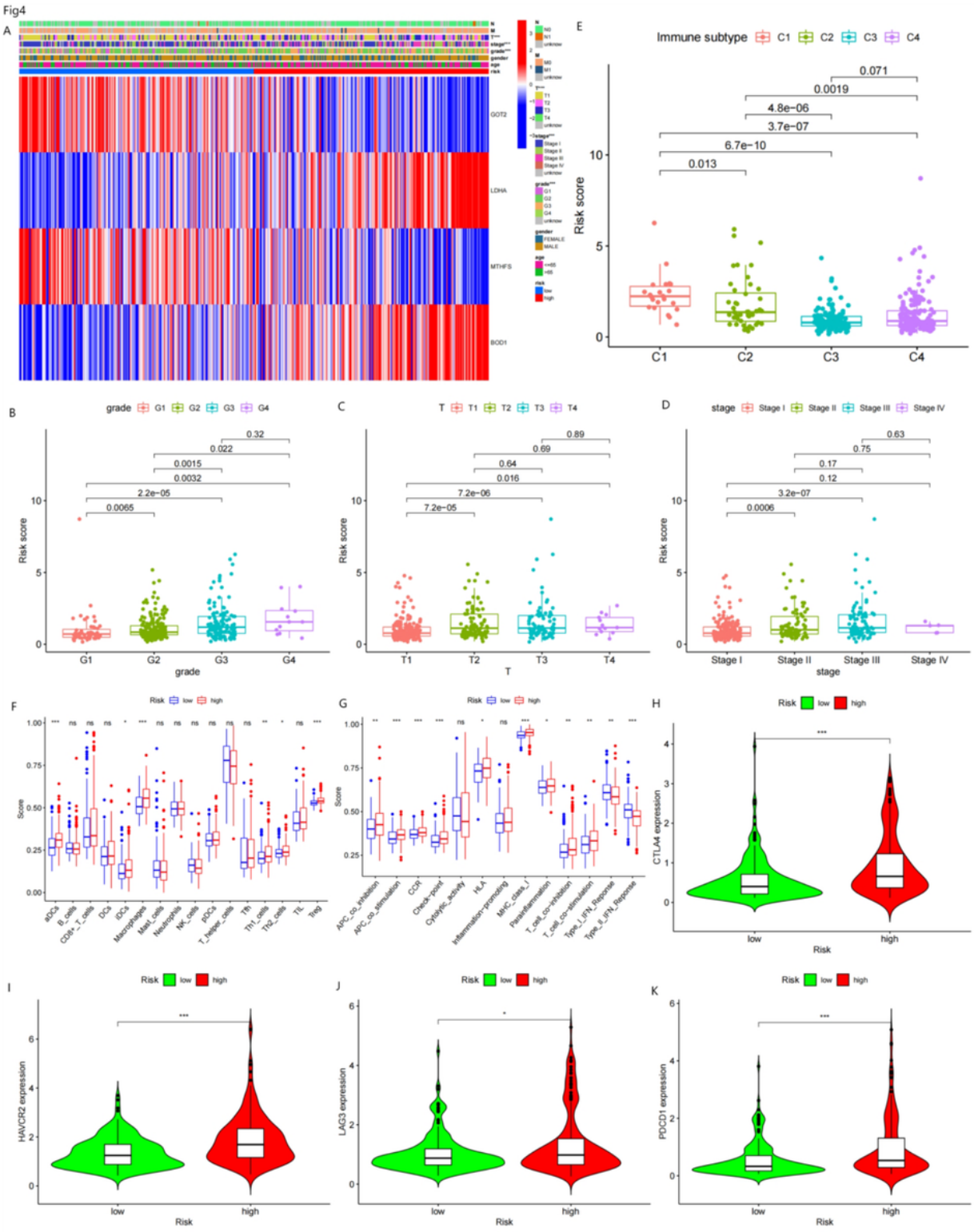

Figure 4

Relationship between risk score, clinicopathologic features and immunity in the TCGA cohort.

A. Heat-map for the connections between clinicopathologic features and the risk groups

B, C, D. Boxplots for risk score among patients with different grade, T, stage

C. Comparison of the risk score in different immune infiltration subtypes.

F, G. Comparison of the enrichment scores of 16 types of immune cells and 13 immune-related pathways between low- and high-risk group

H, I, J, K. High risk scores were positively correlated with up-regulated CTLA4, HAVCR2, LAG3 and PDCD1

Supplementary Files

This is a list of supplementary files associated with this preprint. Click to download.

- supplementtary.zip